# Thermal annealing of carbon nanotubes reveals a strong toxicological impact of the structural defects

Agathe Figarol, Jérémie Pourchez, Delphine Boudard, Valérie Forest, Sarah Berhanu, Jean-Marc Tulliani, Jean-Pierre Lecompte, Michèle Cottier, Didier Bernache-Assollant, Philippe Grosseau

J Nanopart Res (2015) 17:194
DOI 10.1007/s11051-015-2999-0

RESEARCH PAPER

# Thermal annealing of carbon nanotubes reveals a toxicological impact of the structural defects

**Agathe Figarol · Jérémie Pourchez · Delphine Boudard · Valérie Forest · Sarah Berhanu · Jean-Marc Tulliani · Jean-Pierre Lecompte · Michèle Cottier · Didier Bernache-Assollant · Philippe Grosseau**

Received: 6 January 2015 / Accepted: 8 April 2015 / Published online: 22 April 2015


**Abstract** The biological response to pristine and annealed multi-walled carbon nanotubes (MWCNT) was assessed on murine macrophages (RAW 264.7). First, the physicochemical features of the as-produced MWCNT and annealed at 2125 °C for 1 h were fully characterized. A decrease in structural defects, hydrophobicity and catalytic impurities was detected after annealing. Thereafter, their impact on cytotoxicity, oxidative stress, and pro-inflammatory response was investigated at concentrations ranging from 15 to 120 μg $mL^{-1}$. No effect of the 2125 °C treatment was detected on the cytotoxicity. In contrast, the annealed carbon nanotubes showed a significant increase of the pro-inflammatory response. We assumed that this behavior was due to the reduction in structural defects that may modify the layer of adsorbed biomolecules. Surprisingly, the purification of metallic catalysts did not have any significant impact on the oxidative stress. We suggested that the structural improvements from the 2125 °C treatment can decrease the carbon nanotube scavenging capacity and thus allow a higher free radical release which may counterbalance the decrease of oxidative stress due to a lower content of metallic impurities.

**Electronic supplementary material** The online version of this article (doi:10.1007/s11051-015-2999-0) contains supplementary material, which is available to authorized users.

A. Figarol · P. Grosseau
SPIN-EMSE, CNRS: UMR 5307, LGF, Ecole Nationale Supérieure des Mines, 42023 Saint-Étienne, France

A. Figarol (✉) · J. Pourchez (✉) · V. Forest · D. Bernache-Assollant
CIS-EMSE, EA 4624, SFR IFRESIS, LINA, Ecole Nationale Supérieure des Mines, 42023 Saint-Étienne, France
e-mail: figarol@emse.fr

J. Pourchez
e-mail: pourchez@emse.fr

D. Boudard · M. Cottier
EA 4624, SFR IFRESIS, LINA, Université Jean Monnet Saint-Etienne, 42023 Saint-Étienne, France

S. Berhanu
Centre des Matériaux, CNRS UMR 7633, Armines - Mines ParisTech, 91003 Evry, France

J.-M. Tulliani
Department of Applied Science and Technology, Politecnico di Torino, 10129 Turin, Italy

J.-P. Lecompte
SPCTS, Centre Européen de la céramique CNRS: UMR 7315, 87068 Limoges, France

**Keywords** Carbon nanotubes · Annealing · High temperature treatment · Oxidative stress · Inflammation · Defects · Environmental and health effects

**Abbreviations**

| | |
|---|---|
| B.E.T. | Brunauer–Emmet–Teller method |
| CNT | Carbon nanotubes |
| CNTa | Annealed carbon nanotubes |
| CVD | Chemical vapor deposition |
| DCF | 2′,7′-Dichlorodihydrofluorescein |
| DMEM | Dulbecco's Modified Eagle's Medium |
| FEG-SEM | Field-emission gun-scanning electron microscopy |
| HR-TEM | High-resolution transmission electron microscopy |
| $H_2$DCF-DA | 2′7′-Dichlorodihydrofluorescein |
| LDH | Lactate dehydrogenase |
| MWCNT | Multi-walled carbon nanotubes |
| ROS | Reactive oxygen species |
| TDS | Thermal desorption |
| TNF-α | Tumor necrosis factor α |
| XPS | X-ray photoelectron spectroscopy |
| XRD | X-ray diffraction |

## Introduction

Carbon nanotubes (CNT) have received a great deal of attention since their full description in the early 1990s (Iijima 1991). CNT have demonstrated high electric and thermal conductivity, exceptional mechanical resistance, and adsorption capacity leading to numerous studies in academic and industrial research (Baughman et al. 2002; De Volder et al. 2013). However, CNT are classified as inhalable fibers due to their small aerodynamic diameter. Common public opinion associates their morphological resemblance to asbestos fibers and this raises health concerns. Based on the scientific literature, the biological impact of inhaled CNT remains uncertain, but it has been shown that this nanomaterial has the capacity to trigger pathogenic pathways. In vivo studies in rats and mice have reported evidences of inflammation, formation of granulomas, fibrotic structures, and oxidative stress (Muller et al. 2005; Shvedova et al. 2008; Porter et al. 2010). Similarly, cell exposure to CNT could trigger cytotoxicity, pro-inflammatory response, and oxidative stress (Brown et al. 2007; Shvedova et al. 2009; Fröhlich et al. 2012). Nonetheless, available data are still fragmentary and often contradictory. The use of different biological models and toxicity assessment methodologies, as well as the lack of full physicochemical data in nanotoxicology studies can, at least partially, explain the contrasting findings. Thus, one of the main keys to improve our understanding of CNT toxicity is to design specific toxicological works in order to accurately examine the biological impact of given physicochemical features (Jiang et al. 2009; Kayat et al. 2011; Schrurs and Lison 2012).

Surface treatments of the as-produced CNT change their properties and enlarge their potential applications. High temperature treatment, also called thermal annealing or graphitization, has been well documented as a way to improve the purity (i.e. decrease of metallic impurity content) and structural order of multi-walled carbon nanotubes (MWCNT). Common production techniques of MWCNT such as chemical vapor deposition (CVD) require the use of metallic nanoparticles as catalysts. As a result, metal residues are classically found entrapped in MWCNT or on their surface. Moreover, these MWCNT are non-perfect cylindrical graphene sheets and exhibit structural defects in crystalline lattices mainly associated to $sp^3$ carbon hybridization (Ebbesen and Takada 1995). According to Bougrine et al. (2001), annealing MWCNT at 1600 °C under argon reduces the level of metallic impurities due to the vanishing of metal particles. Besides, over 1600 °C, the carbon interlayer spacing starts to contract, with better results obtained at 2400 °C. Boncel and Koziol (2014) suggested that metallic impurities gradually escape as vapors through one CNT open end at a temperature for which a sufficiently high vapor pressure of metal is achieved. Chen et al. (2007) confirmed this purification and structural enhancement with a threshold value of 1800 °C. Heat treatment time was prolonged from 2 to 60 min at the maximum temperature. They stated that the effect of duration time was much lower than that of annealing temperature. Enhancement of MWCNT crystallinity appears to improve their electric conductivity, which could be of great interest for microelectronic or biomedical applications (Fiorito et al. 2009). Similarly, their axial strength and Young's modulus are improved, encouraging the development of high

performance composite material (Pinault et al. 2004; Yamamoto et al. 2013).

Nowadays, the availability of annealed MWCNT on the market is increasing while their effects on health are still not fully understood. In fact, Fiorito et al. (2009) compared MWCNT purified by acid functionalization or by annealing at 2400 °C and concluded that the latter were less cytotoxic but induced a higher pro-inflammatory response on primary human macrophages. Contradicting results from Simon-Deckers et al. (2008) evidenced no impact on the cytotoxicity of human epithelial cells (A549) of MWCNT annealed at 2000 °C compared to raw MWCNT shortened by ultrasonication. Cheng et al. (Cheng et al. 2009) reached a similar conclusion when comparing MWCNT annealed at 2600 °C and raw MWCNT on human monocyte-derived macrophages (HMM). A more complete study was published as two companion papers (Fenoglio et al. 2008; Muller et al. 2008) and assessed the physicochemical and biological effects of annealing MWCNT at 2400 °C. In vitro genotoxicity on lung epithelial cells (RLE) seemed to be slightly reduced by this thermal treatment. A decrease in cytotoxicity and inflammation was furthermore observed in vivo in Wistar rats after intra-tracheal instillations (2 mg/rat). However, high levels of cytotoxicity were observed again after a 6 h grinding. Fenoglio et al. (2008) and Muller et al. (2008) suggest thus that the positive effect on cytotoxicity and pro-inflammatory response was mainly occasioned by the decrease in surface reactive sites due to the higher structural order. Unfortunately, the effects on oxidative stress have not been directly studied as a cellular response. However, in cell-free conditions, annealed MWCNT demonstrated a lower scavenging capacity of the oxygen radicals (Fenoglio et al. 2008; Muller et al. 2008). Furthermore, no MWCNT directly generated any oxidative species. The scavenging activity of CNT corresponds to their "antioxidant" capacity. Thus, it lowers the concentration of reactive oxygen species (ROS) of the surrounding medium. This activity has been shown to be enhanced by lattice defects (Fenoglio et al. 2006, 2008; Galano et al. 2010). To the best of our knowledge, few studies have been conducted to examine the impact of the oxidative stress of the CNT purification by an annealing treatment. Frequently, a causal link between metallic impurities and oxidative stress has been suggested (Kagan et al. 2006; Shvedova et al. 2012; Ge et al. 2012; Bussy et al. 2012). Fe is often used as a catalyst for CNT production and is implicated in the Fenton reaction: $H_2O_2 + Fe^{2+} \rightarrow OH\cdot + Fe^{3+} + OH^-$ (Kagan et al. 2006; Shvedova et al. 2012; Ge et al. 2012). Bussy et al. (2012) exposed a mechanism of release of Fe impurities in the acidic lysosomes after cellular uptake of CNT in murine macrophages. Al, another metallic catalyst, is a non-redox-active metal; however, it can have a strong pro-oxidant activity (Exley 2004; Mahdi et al. 2010; Ruipérez et al. 2012). Al-superoxide could indeed stabilize ferrous ion by reducing its rate of oxidation. It thus indirectly promotes the production of ROS with the use of the ferrous ions in the Fenton reaction. Furthermore, Zhang et al. (2011) compared the cellular response of HeLa cells exposed to MWCNT annealed at 2400 °C, oxidized by a $HNO_3$ treatment or irradiated with $^{60}Co$. Annealed MWCNT exhibited a lower level of structural defects than oxidized or irradiated MWCNT. The induced oxidative stress and cytotoxicity were also lower for annealed CNT. Liu et al. (2011) focused on the acellular activity of an antioxidant, the glutathione (GSH). All the studied carbon-based nanomaterials, including CNT, were linked with a dose-dependent decrease of GSH concentration in the acellular medium. With annealed carbon black (at 2600 °C), however, the final GSH concentration was higher than with pristine carbon black. These two studies suggest a relationship between structural defect and oxidative stress.

Further studies have assessed the biological response toward annealed MWCNT but without any comparison to raw MWCNT. Hirano et al. (2008) showed a high cytotoxicity of MWCNT annealed at 2600 °C which was not linked to apoptosis or oxidative stress, along with a low inflammation. Data from Tsukahara and Haniu (2011) also indicated a dose-dependent cytotoxicity with no sign of apoptosis and oxidative stress, although some cytokines levels were increased (IL-6 and IL-8 but not TNF-α, IL-1β, IL-10, and IL-12) indicating a medium pro-inflammatory response.

Overall, few toxicological studies are available with full comparison of pristine and annealed MWCNT and results are contradictory with very few studies on oxidative stress. In the present work, characterization and in vitro biological assessments of the role of metallic impurities and structural defects were conducted on the as-produced and annealed MWCNT at 2125 °C.

## Experimental procedures

### Powders and thermal annealing treatment of MWCNT

MWCNT (Nanocyl NC7000, Rue de la Vacherie 236, Auvelais, Belgique) were synthesized by CVD and have a diameter of 9.5 nm and a length of 1.5 μm according to the manufacturer. The as-produced MWCNT were labeled CNT. For the annealing treatment, these CNT were allowed to degas under vacuum overnight then were heated at 10 °C $min^{-1}$ until 200 °C and remained at this temperature for 5 h under vacuum and 18 h under argon. The annealed treatment started then, with a heating rate of 10 °C $min^{-1}$ until the maximal temperature of 2125 °C was reached and hold for 1 h. The resulting annealed carbon nanotubes were labeled CNTa. All weighing and the maximum of dried powder manipulations were conducted under an extractor hood in an enclosed laboratory at low pressure.

### Physicochemical characterization of MWCNT

Field-emission scanning electron microscopy (FEG-SEM, JEOL JSM 6500F, Akishima, Tokyo, Japan) at 2 kV was used to characterize the CNT morphology and diameter. A few milligrams of MWCNT powder were put on a carbon-coated holey film. Samples were coated with a 3-nm gold layer before FEG-SEM observations. 100 MWCNT diameters per picture were measured by means of ImageJ software (three pictures were used for a total of 300 measurements). The enhancement in structural order was monitored by Raman spectroscopy (XploRA, Horiba Scientific, rue de Lille, Villeneuve d'Ascq, France) on dry powder. A laser at 532 nm, a ×50 objective, and 20 acquisitions of 20 s were used with, first, a 1200 T network for a spectra between 200 and 3000 $cm^{-1}$, then a 2400 T network, giving a spectra between 1000 and 2000 $cm^{-1}$ for the $I_d/I_g$ characterization. Two usual bands are indeed typical of CNT. The D-band intensity (D for disorder) is linked to the $sp^3$ hybridized carbon, and increases with ill-organized graphite structure (Belin and Epron 2005). The G-band (G for graphite) corresponds to a splitting of the $E_{2g}$ stretching mode of graphite and is independent of the structural defects. Therefore, the ratio of both intensities $I_d/I_g$ informs on the level of structural defects. $I_d/I_g$ values are the mean of at least four measurements. Diameters and CNT morphology were moreover analyzed by high-resolution transmission electron microscopy (HR-TEM). HR-TEM images were acquired on a Tecnai F20 ST microscope (FEI Company) operating at 200 kV with a field-emission gun as the electron source. The samples were prepared by dispersion in ethanol and subsequent ultrasonication. A small amount of the dispersion was then deposited on a TEM copper grid coated with a holey carbon film (Agar Scientific, Elektron Technology UK Ltd, Stansted, Essex, CM24 8GF, UK). The specific surface area (SSA) was determined by $N_2$ adsorption at 77 K after out-gassing for 4 h at 110 °C (Micromeritics ASAP 2000, Micromeritics Corporate Headquarters, 4356 Communications Dr., USA) using the Brunauer–Emmet–Teller (B.E.T.) method. The purification from metallic impurities was assessed by inductively coupled plasma atomic emission spectroscopy (ICP-AES) identifying trace metals after mineralization by nitro-hydrochloric acid. Furthermore, to fully characterize the MWCNT, X-ray photoelectron spectroscopy (XPS) was used to analyze the surface chemistry. The oxygen atomic percentages were obtained by analyzing the ratio between the intensities of the $O_{1s}$ and $C_{1s}$ XPS peaks (with 20 % incertitude, monochromatized Al $K_\alpha$ source, 400 μm width analyzed, $1.3 \times 10^{-7}$ Pa of residual pressure, Thermo VG ThetaProbe, Thermo Fisher Scientific Inc., Wyman Street, Waltham, USA). Samples were prepared by the sonication of a 30 μg $mL^{-1}$ CNT suspension in ethanol (5–15 min, 24 W $mL^{-1}$, 3 mm probe, Branson Sonifier SD450, Parc d'Affaires Silic, Rungis, France). One drop was deposited and dried on a 1 $cm^2$ silicon wafer previously covered by a thin layer of gold. The spectra were corrected for Shirley-type backgrounds. Automatic search of the peak positions was conducted from the fixed C1s peak at 284.5 eV. Atomic percentages were calculated from the peak areas and given sensitivity factors. Assessment of the surface chemistry was completed by thermal desorption spectroscopy (TDS, supplementary data—Fig. S1). 10 mg of powder was heated under vacuum at a heating rate of 20 °C $min^{-1}$ until 850 °C. Two turbomolecular pumps ensure a vacuum of less than $10^{-2}$ Pa from air atmosphere. A mass spectrophotometer (Balzers QMG 112 quadrupole, Iramali 18, Balzers, Liechtenstein) collected and analyzed the volatilized elements. Zeta potentials were measured

using a Zetasizer Nano ZS (Malvern Instruments) and 30 μg $mL^{-1}$ carbon nanotubes suspensions in deionized water or culture medium prepared by sonication (5 min, 24 W $mL^{-1}$, 3 mm probe, Branson Sonifier).

Preparation of MWCNT suspensions for the toxicity assays

0.80 mg of MWCNT was weighed and dispersed in 5 mL of culture medium: Dulbecco's Modified Eagle's Medium (DMEM, Invitrogen, Carlsbad, CA, USA) supplemented with 10 % of fetal calf serum (Invitrogen), and 1 % penicillin–streptomycin (penicillin 10,000 U $mL^{-1}$, streptomycin 10 mg $mL^{-1}$, Sigma-Aldrich, Saint-Louis, MO, USA). A 5-min sonication was performed to fully disperse each MWCNT sample (3 mm probe, 24 W $mL^{-1}$, Branson Sonifier S-450D). Serial dilutions were conducted to obtain concentrations of 160, 80, 40, and 20 μg $mL^{-1}$ of MWCNT in supplemented culture medium DMEM. For the toxicity assays, 25 μL of cell suspension was supplemented by 75 μL of the MWCNT suspension (1/4 cells, 3/4 MWCNT). The final concentrations were 120, 60, 30, and 15 μg $mL^{-1}$. The suspension stability over a week was established by dynamic light scattering (ZetaSizer Nano ZS). It measured the average hydrodynamic diameter of the equivalent sphere with a density of 1 with the same translational diffusion coefficient.

In vitro toxicity assays

*Cell culture of RAW macrophages*

RAW 264.7 macrophage cell line was provided by ATCC Cell Biology Collection (Promochem LGC, Queens Road, Teddington, Middlesex, UK). It was derived from mice peritoneal macrophages transformed by the Albeson Murine Leukemia Virus. Cells were grown in 10 % fetal calf serum supplemented DMEM and maintained at 37 °C under a 5 % carbon dioxide humidified atmosphere.

*Cytotoxicity of macrophages after exposure to MWCNT*

The cells were seeded in a 96-well plate at 100,000 cells/well and incubated with the MWCNT for 24 h. Cell viability was then evaluated by quantifying the Lactate dehydrogenase (LDH) released from cells with damaged membranes using the CytoTox-96® Non-radioactive Cytotoxicity Assay (Promega, Woods Hollow Road, Madison, USA) according to the manufacturer's instructions. Detection was performed using a microplate reader (Multiskan GO, Thermo Fisher Scientific Inc., Wyman Street, Waltham, USA) at 450 nm. The amount of released LDH was reported as a percentage of the total cellular LDH (measured after the complete lysis of control cells).

*Pro-inflammatory response of macrophages after exposure to MWCNT*

In parallel to the cytotoxicity test, 100,000 cells/well were seeded in a second 96-well plate and incubated with the MWCNT for 24 h. Tumor necrosis factor alpha (TNF-α) release was assessed using a commercial enzyme-linked immunosorbent assay kit (Quantikine® Mouse TNF-α/TNFSF1A Immunoassay, R&D systems Inc., McKinley Place NE, Minneapolis, USA). The optical density was determined according to the manufacturer's instructions, using a microplate reader (Multiskan GO, Thermo Scientific) at 450 nm. A standard curve was established and results were expressed in pg $mL^{-1}$ of TNF-α.

*Oxidative stress of macrophages after exposure to MWCNT*

Acute oxidative stress was determined by measuring the level of intracellular ROS by the OxiSelect™ Intracellular ROS Assay Kit (Cell Biolabs). Briefly, the cells were seeded at $2 \times 10^6$ cells/well and allowed to adhere in a black 96-well plate for 4 h. A 1 h pre-treatment with the cell-permeant 2′7′-dichlorodihydrofluorescein ($H_2$DCF-DA) was carried out before a 90-min exposure to the MWCNT. The fluorescence intensities were read at 480 nm excitation and 530 nm emission (Fluoroskan Ascent, Thermo scientific). A positive control with cells exposed to 1 mM $H_2O_2$ was added. Biases were found to result from the fluorescence absorption by the black MWCNT. Results were thus corrected by the mean of cell-free standard curves. They were traced after the variation of the fluorescent intensity of known concentrations of DCF probe (2′,7′-dichlorodihydrofluorescein) in complemented medium with and without MWCNT and without cells. Corrections of

artifacts were calculated and applied for each CNT type and each dose (Supplementary data—Fig. S2 and Table S1).

*Statistical analysis*

Results were expressed as the mean of three independent experiments, each carried out in triplicates, with standard errors of the mean value. Statistical significance was declared when $p < 0.05$ using a Student test with Tanagra software (Rakotomalala 2005).

## Results

Physicochemical features

*Morphology and specific surface area of the MWCNT*

A thorough characterization of the nanomaterials is crucial. FEG-SEM images are presented in Fig. 1. The morphology of the MWCNT remained alike after heating at 2125 °C, presenting entangled tubes with no or very few traces of amorphous carbon. As shown in Table 1, where all physicochemical features are summarized, the mean diameter was not impacted, nor was the diameter distribution (see Supplementary Data—Fig. S3). The results were confirmed by HR-TEM measurements: 17 ± 5 nm for CNT by SEM and HR-TEM, 17 ± 5 nm and 18 ± 4 nm for CNTa by SEM and HR-TEM, respectively (Fig. 2). While the measured mean diameter is almost twice the diameter given by the producer, the entanglement of the tubes unfortunately did not allow to confirm the given length of 1.5 µm. The nanotube structure was more specifically assessed by HR-TEM before and after the annealing treatment (Fig. 2). HR-TEM revealed some significant variation between nanotubes coming from the same sample, both for untreated and annealed CNT. For instance, the number of inner walls ranged from 3 to more than 20 depending on the individual nanotube under consideration. The crystalline quality also varied significantly between nanotubes forming one sample. Typical defects such as kinks, wavy tubes, surface roughness, or "bamboo-type" inner structures were observed for both CNT and CNTa. However, the number of metallic impurities due to catalyst particles located inside the tubes greatly decreased after the annealing procedure. Moreover, CNTa tended to exhibit less surface roughness, indicating that the annealing treatment had slightly improved the nanotube crystalline quality. No significant change due to the thermal annealing area was detected in the SSA.

*Lattice defects of the MWCNT*

Raman spectroscopy was used to assess the lattice defects of the two MWCNT. The spectra exhibited the two typical bands of carbon material: the D-band (1340 $cm^{-1}$) and the G-band (1575 $cm^{-1}$), with two overtone peaks: the D'-band (2685 $cm^{-1}$) and the G'-band (2930 $cm^{-1}$) (Fig. 3 is an illustration of one

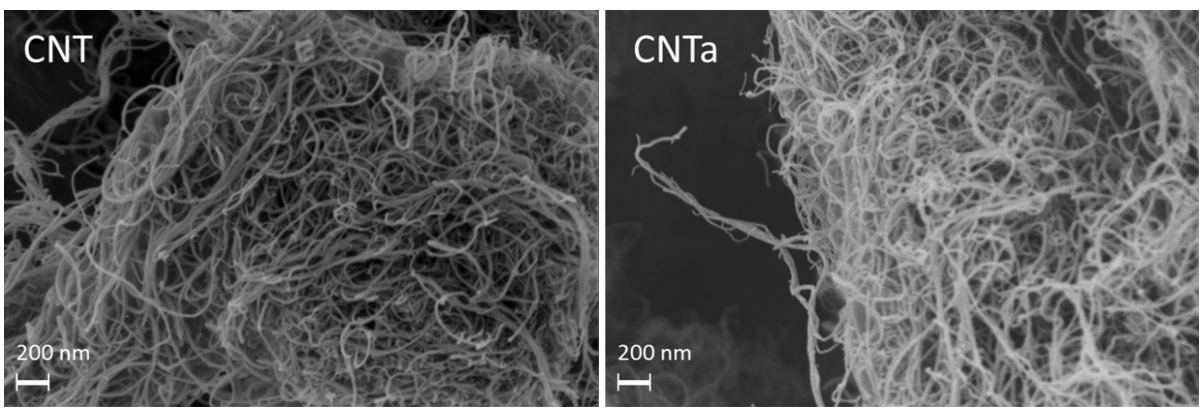


**Fig. 1** FEG-SEM images of multi-walled carbon nanotubes: as-produced (CNT) and after an annealing treatment at 2125 °C under Ar (CNTa)

**Table 1** Physicochemical characteristics of the two carbon nanotubes

| Sample | CNT | CNTa |
|---|---|---|
| Diameter (nm) | 17 ± 5 | 17 ± 5 |
| Structural disorder ($I_d/I_g$) | 1.18 ± 0.10 | 0.77 ± 0.13 |
| SSA ($m^2$ $g^{-1}$) | 212 ± 3 | 209 ± 3 |
| Catalytic impurities (wt%) | Fe 0.19 | Fe 0.01 |
| | Al 4.23 | Al 0.00 |
| | Co 0.12 | Co 0.00 |
| O (atomic proportion %) | 8.7 | 3.5 |
| Zeta potential in water (mV) | −23.3 ± 7.0 | −36.4 ± 4.3 |
| Zeta potential in culture medium (mV) | −127.0 ± 8.6 | −156.0 ± 6.6 |

*CNT* as-produced MWCNT, *CNTa* MWCNT annealed at 2125 °C under Ar. Mean diameters were determined by FEG-SEM observations and confirmed by HR-TEM. $I_d/I_g$ corresponds to the intensity ratio of the Raman D and G-bands. *SSA* specific surface area, measured according to Brunauer Emmett and Teller protocol. Catalytic impurity level was assessed by ICP-AES, levels <0.01 wt% were found for Cu, Cr, Ni, and Ti. O/C atomic proportion is the intensity ratio of the $O_{1s}$ and $C_{1s}$ XPS peaks

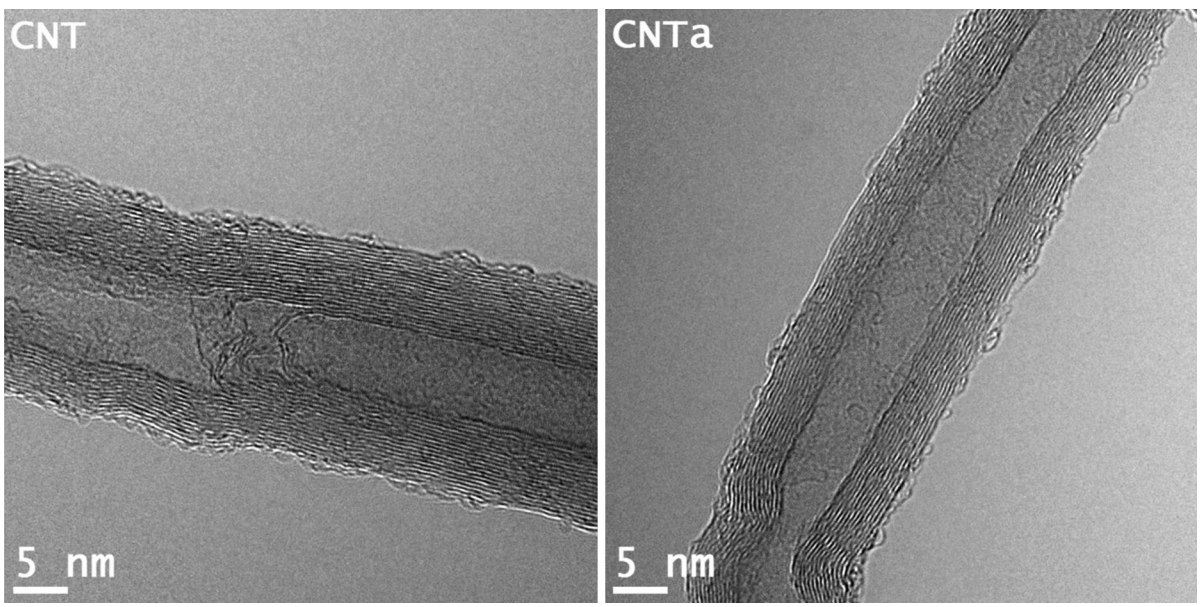


**Fig. 2** HR-TEM images of multi-walled carbon nanotubes: as-produced (CNT) and after an annealing treatment at 2125 °C under Ar (CNTa)

Raman measurement). The $I_d/I_g$ ratio was significantly lowered by the annealing treatment from 1.24 to 0.77 which notifies of a higher crystallinity degree without a complete disappearance of the structural defects however. X-ray diffraction (XRD) was performed to further analyze the crystallinity of the samples. No change was, however, detectable between the two XRD diffraction patterns (see Supplementary Data—Figs. S4 and S5).

*Purification after annealing treatment of CNTa*

As expected, the 2125 °C treatment removed all metallic impurities. It was quantitatively confirmed by ICP-AES since all traces of Fe, Al, and Co disappeared (Table 1). Al was the main catalyst used to produce those MWCNT and its level fell from 4.23 wt% to an undetectable value (<0.01 wt%). The

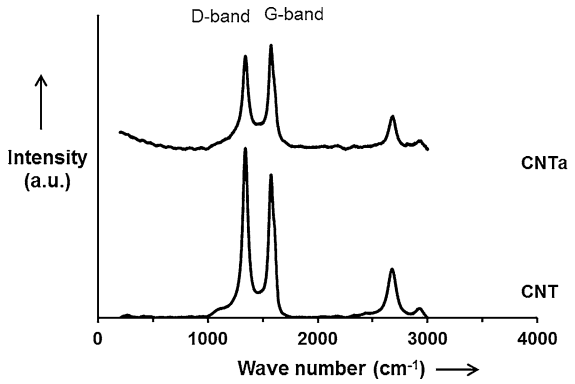


**Fig. 3** Raman spectra of carbon nanotubes: as-produced (CNT) and after an annealing treatment at 2125 °C under Ar (CNTa)

HR-TEM images allowed to qualitatively confirm the presence of metal content before the annealing treatment and their disappearance after it (supplementary data—Fig. S6).

*Chemical modifications after annealing treatment of CNTa*

The surface oxygen content was assessed by XPS analysis. First, general XPS spectra were analyzed for both samples (supplementary data—Fig. S7). Three main peaks were identified: the C1s peak at 284.5 eV, the O1s peak at 533 eV, and the Au 4f peaks from the substrate at 84 and 87.5 eV. The absence of contribution from the $SiO_2$ substrate (no signal from the Si2p peak) was verified. A more detailed spectrum was recorded for each of the four peaks. The O/C atomic proportions (in percentage) are given in Table 1. The amount of oxygen decreased after the annealing treatment. The heating has probably desorbed and decomposed the oxygen-containing groups which were present at the nanotubes surface. Further assessment of the surface chemistry was conducted by the analysis of zeta potentials and TDS. TDS results showed a decrease in overall oxygenated groups especially with the disappearance of the peak due to physisorption (in the 0–200 °C range) (Fig. 4). A peak due to chemisorption of oxygenated groups (in the 400–600 °C range, Xia et al. 2007) appeared after the annealing treatment and seemed to have been masked by the overall higher level of oxygenated groups. $CO_2$ and $H_2O$ desorptions confirmed the decrease of those oxygenated groups (see Supplementary data—Figs. S8 and S9). Zeta potentials in deionized water and culture medium are presented in Table 1. The observed decrease in zeta potential in water is quite surprising. The pH of the suspensions was close enough ($4.9 \pm 0.6$ and $4.8 \pm 0.1$) so that the difference should not contribute to the difference in zeta potentials. On the other hand, suspensions in buffered culture medium were stable. Zeta potentials were very low, but the zeta potential of this culture medium alone (complemented DMEM) was already $-100$ mV $\pm 12$. The difference in zeta potentials in culture medium could be due to the difference in the profile of the proteins at the CNT surface.

Biological toxicity assessed in macrophages

The interaction of the MWCNT and the macrophages was confirmed by microscopic observations (Supplementary data—Fig. S10). These pictures allow to assess the final size of CNT and CNTa agglomerates in culture medium. CNT tended to exhibit less and smaller agglomerates than CNTa: average of 2.2 μm ± 0.7 for CNT and 3.5 μm ± 1.9 for CNTa (with some of the agglomerates as big as 10 μm).

*Cytotoxicity*

LDH released from cells with damaged membranes, if significantly higher than the negative controls, is an indicator of cytotoxicity. For both MWCNT, a significant LDH release was uniquely observed at the maximum dose of 120 μg $mL^{-1}$ (Fig. 5). No significant difference was found between the cytotoxicity induced by CNT or CNTa.

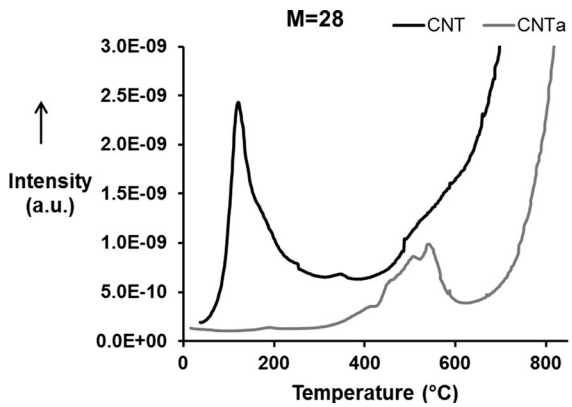


**Fig. 4** Thermal desorption of carbon nanotubes, following the $M = 28$ related to CO. CNT: MWCNT as-produced, CNTa: MWCNT after an annealing treatment at 2125 °C under Ar

*Pro-inflammatory response*

TNF-α is one of the cytokines indicators of the pro-inflammatory response for macrophage cells. The annealing treatment seemed to significantly increase the TNF-α production (Fig. 6). It was found significant only at the highest concentration of CNT, while the levels were significant from 60 μg $mL^{-1}$ of CNTa with a dose-dependent response.

*Oxidative stress*

Measurement of ROS production demonstrated a significant high dose response for both MWCNT, sign of a high oxidative stress (Fig. 7). No significant difference was observed after the annealing treatment. The levels were already significant before corrections of the bias induced by the CNT absorption of fluorescence (at comparable levels with the positive control). After correction, the response was magnified with ROS levels reaching three times the level of the positive control.

## Discussion

### Impact of the thermal annealing on the physicochemical features

The main originality of this study was to be specifically designed in order to assess the impact of the lattice defects and metallic impurities on the macrophage

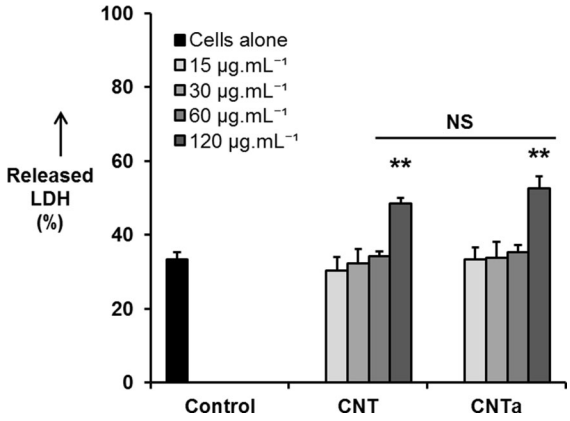


**Fig. 5** Cytotoxicity induced by a 24 h exposure to MWCNT as-produced (CNT) and annealed at 2125 °C (CNTa). Significantly different from negative control, $^{**}p < 0.001$. *NS* not significantly different between CNT and CNTa

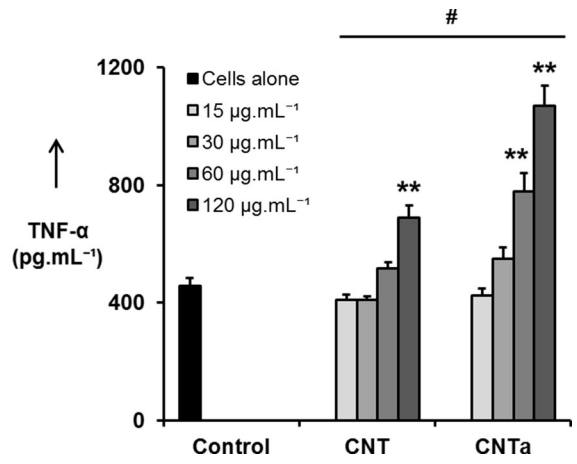


**Fig. 6** Pro-inflammatory response of macrophages after a 24 h contact with the as-produced MWCNT (CNT) and annealed at 2125 °C MWCNT (CNTa). Significantly different from the negative control, $^{**}p < 0.001$, $^{\#}$significantly different between CNT and CNTa, $p < 0.01$ at 30 μg $mL^{-1}$, $p < 0.001$ at 60 and 120 μg $mL^{-1}$, and not significantly different at 15 μg $mL^{-1}$

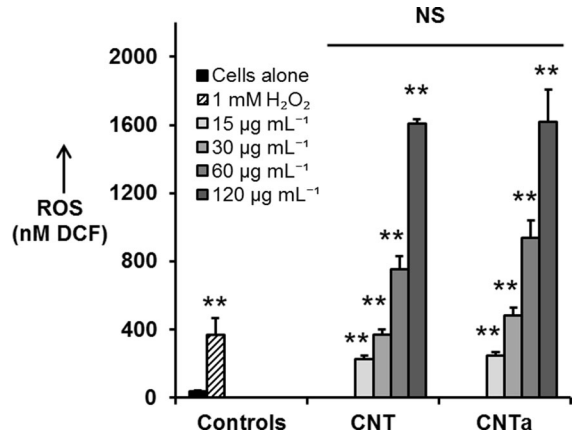


**Fig. 7** Reactive oxygen species (ROS) production by murine macrophages after a 90 min exposure to MWCNT as-produced (CNT) and annealed at 2125 °C (CNTa) after correction of fluorescent decrease by MWCNT. Significantly different from negative control, $^{**}p < 0.001$. *NS* no significant difference between CNT and CNTa

in vitro response. First, the physiochemical features were evaluated before and after a 2125 °C treatment. The measured mean diameters were found to be twice the value from the producer. Detecting the diameter of CNT bundles rather than isolated CNT could modify the measurement (Peigney et al. 2001). However, HR-TEM measurements allowed a better precision by

selecting isolated CNT and still confirmed the mean diameter. We were not able to measure the CNT length, but according to Yamamoto et al. (2013) if an annealing treatment could slightly reduce the CNT diameter, no impact was detected on the length. While no change was induced neither in the diameter and diameter distribution, nor on the SSA; the amount of lattice defects and catalytic impurities were decreased by heating at 2125 °C, as shown by Raman spectroscopy, ICP-AES and HR-TEM. Our ICP-AES data showed a removal of 4.5 wt% metallic impurities, so the change in specific area should be 0.05 % but the difference is not sufficient to be detected by B.E.T. method. Chen et al. (2007) were able to observe some differences in the X-ray diffraction patterns before and after annealing, as the peaks were sharper and more defined. However, for a maximal temperature of 2000 °C, the differences in XRD patterns were minimal; they were more evident after annealing over 2200 °C. In our study, the maximum temperature reached was 2125 °C, which might explain why no change was seen in the XRD patterns. The crystalline lattice enhancement, thus the diminution of reactive sites, was correlated to a decrease of oxygen-containing groups as revealed by the XPS and TDS. Moreover, metal oxides strongly bind hydrophilic groups. Therefore, the purification from Al and Fe may also contribute to the decrease of oxygen-containing groups (Fubini et al. 1999; Fenoglio et al. 2008). The level of oxygen-containing groups remained, however, still a relatively high content. This could be linked to the structural defects that still remained after annealing, favoring the adsorption of a thin layer of oxygen-containing groups with a passivation mechanism. The presence of this thin layer could explain why the zeta potential in water was lower after annealing, while the XPS and TDS measurement showed a lower content of oxygen-containing groups. Zeta potential is indeed a measurement of the very external charge of the CNT. Furthermore, the decrease of physisorbed water observed by TDS is a clear indication that the annealing treatment increased the hydrophobicity of the CNTa. Microscopic observations are representative of the agglomeration trend. CNT tended to exhibit less and smaller agglomerates, which is coherent with the increase in hydrophobicity after annealing.

### Impact of the thermal annealing on the in vitro biological response

Concentrations of 15–120 μg $mL^{-1}$ (3.75–30 μg $cm^{-2}$) were chosen within the range of commonly used doses (Simon-Deckers et al. 2008; Tsukahara and Haniu 2011). Regarding potential human exposure, Vietti et al. (2013) considered these doses as pertinent even though overestimated. The overestimation counterbalances the short exposure, the irregular CNT distribution in lung, and the low deposition in vitro decreasing the effective dose in contact with the cells.

No effect of the annealing treatment was observed regarding LDH leakage. The cytotoxicity seemed thus not to be linked with the two principal physicochemical characteristics modified by the annealing treatment: the lattice defects and the metallic impurity content. This suggests that these two parameters have no direct influence on the loss of membrane integrity. These results are consistent with the study of Simon-Deckers et al. (2008). Muller et al. (2008) found on the contrary that the annealing treatment when carried out after a 6 h grinding step decreases the LDH leakage, compared to just grinded CNT. However, after a low thermal treatment at 600 °C, the cytotoxicity was already decreased. The observed difference may thus not result from the metallic purification and structural enhancement. Moreover, the study design was radically different. This was an in vivo study with 2 mg of MWCNT administered intratracheally to Wistar rat. The LDH assay was realized on the bronchoalveolar lavage supernatant recovered 3 days after exposure, so the results are not comparable to our study.

An increase in TNF-α production was detected after the annealing treatment. The metallic purification and reduction of structural defects did not have any protective effect to the pro-inflammatory response. On the contrary, a decrease in structural defects may increase the inflammation through the increase of hydrophobicity or the modification of the protein corona at the CNT surface. Fenoglio et al. (2008) acknowledged indeed a relationship between structural defects and water interaction, with an increase of the hydrophobicity after annealing. It was suggested here by the TDS and XPS measurements that the annealing treatment increased the hydrophobicity and decreased the level of surface oxygen-containing groups. First, this seemed to have an impact on the size of the agglomerates, secondly

this could impact a potential adsorption of the TNF-α on the CNT, and moreover it can influence the corona layer. Indeed, it is now well known that CNT can interfere with common toxicity tests (Wörle-Knirsch et al. 2006; Casey et al. 2007). In one of our previous work (Forest et al. 2015), we have demonstrated that concerning the LDH measurements, the two main biases observed for this test almost compensated and had no impact on the conclusion. Concerning the ROS assessment, the results were corrected to avoid such biases as explained in the Material and Method part. As for the TNF-α, Leshuai and Zhang (2007) showed that TNF-α could be adsorbed on hydrophilic SWCNT, which may interfere with the ELISA test and lead to an underestimation of the TNF-α level. Pristine CNT could present a higher TNF-α adsorption compared to more hydrophobic CNTa. It could thus explain the lower levels of TNF-α observed for CNT compared to CNTa. However, considering the critical differences in the TNF-α concentration measured for CNT and CNTa, it may be hard to believe that these kinds of biases were the main cause of it. Lynch and Dawson (2008) described in their work the corona model: a layer of biomolecules, mainly proteins, adsorbed to the nanoparticle surface in a dynamic equilibrium. In the context of cell culture, this corona should be composed by the culture medium proteins. Kapralov et al.(2012) then Cai et al. (2013) demonstrated the adsorption of surfactant lipids and proteins on CNT, confirming the presence of protein corona. The protein corona can influence the biological response as the object interacting with the cells is really the CNT and its adsorbed layer (Mao et al. 2013; Lanone et al. 2013). Thermal structural enhancement could influence the protein corona either by a decrease of adsorption sites or by a modification of the nature and conformation of the adsorbed proteins. These changes in surface chemistry could explain potentially the increase in the pro-inflammatory response. Dutta et al. (2007) showed that precoating single-walled CNT with a non-ionic surfactant inhibited albumin adsorption and the CNT anti-inflammatory properties. Therefore, it is possible that the impact of the annealing treatment on the pro-inflammatory response may be due to the change in surface chemistry.

Furthermore, Schinwald et al. (2012) suggested in their study that the threshold length to induce frustrated phagocytosis is 5 μm in mice. In our work, the measured agglomerates have mean length under this threshold. No frustrated phagocytosis was observed here. However, the discussion about lattice defects and corona could also partly explain the higher inflammation caused by rigid CNT. It is thought to be due to the phenomena of frustrated phagocytosis where macrophages fail to fully engulf oversized CNT (Brown et al. 2007; Nagai et al. 2011). Such rigid CNT triggering frustrated phagocytosis are highly crystallized. Thus, the modification of the protective layer could have an additional role in the increase of the inflammation. Again, our results were not consistent with those of Muller et al. (2008). The in vitro and in vivo inflammatory responses were found to be decreased after annealing of the grinded CNT. But again, the biological response was already reduced by half in vivo or to a non-significant level in vitro after a low thermal treatment. Thus, it can be suggested that the effect on the inflammation was not mainly due to structural enhancement or metallic purification.

In the present work, it was first hypothesized that the main impact of high temperature annealing was the decrease in oxidative stress due to the purification from catalytic impurities. However, no decrease of the ROS production was observed after the annealing treatment. Our hypothesis was based on the relationship between metallic impurity content and oxidative stress. It has indeed been suggested that transition metal like Fe (Ge et al. 2012), and indirectly metals such as Al (Ruipérez et al. 2012) contribute to ROS generation. To explain the absence of decrease in ROS production after the CNT purification, a second mechanism has to be taken into account: the CNT-scavenging capacity. CNT seem indeed to have the ability to quench rather than generate oxygenated free radicals. The origin of this mechanism is still under debate; however, it has been shown to decrease after annealing due to the reduction of structural defects (Fenoglio et al. 2006, 2008). The same phenomenon has been observed concerning GSH: before annealing, carbon nanomaterials have the capacity to decrease the level of GSH in the medium (Zhang et al. 2011; Liu et al. 2011); after annealing, the level of GSH increased. The scavenging activity could mask the ROS production and decrease the oxidative stress. Thus, a balance between the reduction of catalytic impurities and the reduction of the scavenging activity could explain why no effect of the annealing treatment was detected regarding the oxidative stress. The CNT-

scavenging activity was not evaluated in this study, and to our knowledge, no other comparative study of the impact on CNT thermal annealing on the oxidative stress has been published. Therefore, this remains a hypothesis that would be further questioned in a complementary study. Besides, it has to be underlined that even the purified CNTa enhanced a high ROS production. This implicates that CNT could trigger oxidative stress independently of metallic impurities. This capacity seems to be linked with the CNT/cell interaction and to be dependent on the CNT physicochemical properties. Tsukahara and Haniu (2011) studied the ROS production in a human bronchial epithelium cell line after a 24 h exposure to 0.1–100 μg $mL^{-1}$ of annealed MWCNT (2800 °C) and found no significant response. They did not assess the content of catalytic impurities and the level of structural defects, but very few amounts were expected. Thus, the absence of oxidative stress could not be due to the scavenging activity, but may be due to the MWCNT characteristics. Likely, in our latest study (Figarol et al. 2014), the oxidative stress of annealed (2600 °C) large MWCNT with high crystallinity and no distinguishable impurities was assessed and no response was found either. We thus suggest that the oxidative stress can be enhanced either by metallic impurities or by the simple presence of CNT, depending on the CNT physicochemical characteristics; and that the oxidative stress can be reduced by the scavenging activity, due to the defects in crystalline lattice.

## Conclusion

Both metallic impurities and structural defects play an important role in the in vitro biological response of CNT. In this study, 2125 °C thermal treatment was used to purify the CNT of catalytic metal content and then to decrease the level of crystalline defects. This annealing treatment showed no influence on the cytotoxicity and the oxidative stress, but revealed an increase of the pro-inflammatory response. Although metallic impurities are supposed to enhance the oxidative stress, we suggest that the impact of the metallic purification is counterbalanced by the decrease of structural defects and thus of the associated scavenging activity. The change in hydrophobicity could moreover modify the nature, number, and conformation of the proteins adsorbed at the CNT surface, and impact the pro-inflammatory process. Further researches could be useful to confirm these assumptions by exploring the possible causal relationship between the protein corona, the scavenging activity and the biological response. Finally, an annealing treatment did not seem to be an appropriate way to decrease the biological response in the case of a safer by design approach.

**Acknowledgments** The authors would like to thank Dominique Goeuriot and Christophe Meunier from the center of structures and materials sciences (EMSE, St-Etienne) for their help regarding the annealing treatment.

## References

Baughman RH, Zakhidov AA, de Heer WA (2002) Carbon nanotubes—the route toward applications. Science 297:787–792. doi:10.1126/science.1060928

Belin T, Epron F (2005) Characterization methods of carbon nanotubes: a review. Mater Sci Eng B Solid State Mater Adv Technol 119:105–118. doi:10.1016/j.mseb.2005.02.046

Boncel S, Koziol KKK (2014) Enhanced graphitization of c-CVD grown multi-wall carbon nanotube arrays assisted by removal of encapsulated iron-based phases under thermal treatment in argon. Appl Surf Sci 301:488–491. doi:10.1016/j.apsusc.2014.02.108

Bougrine A, Dupont-Pavlovsky N, Naji A et al (2001) Influence of high temperature treatments on single-walled carbon nanotubes structure, morphology and surface properties. Carbon 39:685–695. doi:10.1016/S0008-6223(00)00165-2

Brown DM, Kinloch IA, Bangert U et al (2007) An in vitro study of the potential of carbon nanotubes and nanofibres to induce inflammatory mediators and frustrated phagocytosis. Carbon 45:1743–1756. doi:10.1016/j.carbon.2007.05.011

Bussy C, Pinault M, Cambedouzou J et al (2012) Critical role of surface chemical modifications induced by length shortening on multi-walled carbon nanotubes-induced toxicity. Part Fibre Toxicol 9:46. doi:10.1186/1743-8977-9-46

Cai X, Ramalingam R, Wong HS et al (2013) Characterization of carbon nanotube protein corona by using quantitative proteomics. Nanomed Nanotechnol Biol Med 9:583–593. doi:10.1016/j.nano.2012.09.004

Casey A, Herzog E, Davoren M et al (2007) Spectroscopic analysis confirms the interactions between single walled carbon nanotubes and various dyes commonly used to assess cytotoxicity. Carbon 45:1425–1432. doi:10.1016/j.carbon.2007.03.033

Chen J, Shan JY, Tsukada T et al (2007) The structural evolution of thin multi-walled carbon nanotubes during isothermal annealing. Carbon 45:274–280. doi:10.1016/j.carbon.2006.09.028

Cheng C, Müller KH, Koziol KKK et al (2009) Toxicity and imaging of multi-walled carbon nanotubes in human

macrophage cells. Biomaterials 30:4152–4160. doi:10.1016/j.biomaterials.2009.04.019
De Volder MFL, Tawfick SH, Baughman RH, Hart AJ (2013) Carbon nanotubes: present and future commercial applications. Science 339:535–539. doi:10.1126/science.1222453
Dutta D, Sundaram SK, Teeguarden JG et al (2007) Adsorbed proteins influence the biological activity and molecular targeting of nanomaterials. Toxicol Sci 100:303–315. doi:10.1093/toxsci/kfm217
Ebbesen TW, Takada T (1995) Topological and $sp^3$ defect structures in nanotubes. Carbon 33:973–978. doi:10.1016/0008-6223(95)00025-9
Exley C (2004) The pro-oxidant activity of aluminum. Free Radic Biol Med 36:380–387. doi:10.1016/j.freeradbiomed.2003.11.017
Fenoglio I, Tomatis M, Lison D et al (2006) Reactivity of carbon nanotubes: free radical generation or scavenging activity? Free Radic Biol Med 40:1227–1233. doi:10.1016/j.freeradbiomed.2005.11.010
Fenoglio I, Greco G, Tornatis M et al (2008) Structural defects play a major role in the acute lung toxicity of multiwall carbon nanotubes: physicochemical aspects. Chem Res Toxicol 21:1690–1697. doi:10.1021/tx800100s
Figarol A, Pourchez J, Boudard D et al (2014) Biological response to purification and acid functionalization of carbon nanotubes. J Nanoparticle Res 16:1–12. doi:10.1007/s11051-014-2507-y
Fiorito S, Monthioux M, Psaila R et al (2009) Evidence for electro-chemical interactions between multi-walled carbon nanotubes and human macrophages. Carbon 47:2789–2804. doi:10.1016/j.carbon.2009.06.023
Forest V, Figarol A, BOUDARD D et al (2015) Adsorption of lactate dehydrogenase enzyme on carbon nanotubes: how to get accurate results about the cytotoxicity of these nanomaterials. Langmuir. doi:10.1021/acs.langmuir.5b00631
Fröhlich E, Meindl C, Höfler A, et al (2012) Combination of small size and carboxyl functionalisation causes cytotoxicity of short carbon nanotubes. Nanotoxicology 1–14. doi: 10.3109/17435390.2012.729274
Fubini B, Zanetti G, Altilia S et al (1999) Relationship between surface properties and cellular responses to crystalline silica: studies with heat-treated cristobalite. Chem Res Toxicol 12:737–745. doi:10.1021/tx980261a
Galano A, Francisco-Marquez M, Martinez A (2010) Influence of point defects on the free-radical scavenging capability of single-walled carbon nanotubes. J Phys Chem C 114:8302–8308. doi:10.1021/jp101544u
Ge C, Li Y, Yin J-J et al (2012) The contributions of metal impurities and tube structure to the toxicity of carbon nanotube materials. NPG Asia Mater 4:e32. doi:10.1038/am.2012.60
Hirano S, Kanno S, Furuyama A (2008) Multi-walled carbon nanotubes injure the plasma membrane of macrophages. Toxicol Appl Pharmacol 232:244–251. doi:10.1016/j.taap.2008.06.016
Iijima S (1991) Helical microtubules of graphitic carbon. Nature 354:56–58. doi:10.1038/354056a0
Jiang J, Oberdorster G, Biswas P (2009) Characterization of size, surface charge, and agglomeration state of nanoparticle dispersions for toxicological studies. J Nanoparticle Res 11:77–89. doi:10.1007/s11051-008-9446-4
Kagan VE, Tyurina YY, Tyurin VA et al (2006) Direct and indirect effects of single walled carbon nanotubes on RAW 264.7 macrophages: role of iron. Toxicol Lett 165:88–100. doi:10.1016/j.toxlet.2006.02.001
Kapralov AA, Feng WH, Amoscato AA et al (2012) Adsorption of surfactant lipids by single-walled carbon nanotubes in mouse lung upon pharyngeal aspiration. ACS Nano 6:4147–4156. doi:10.1021/nn300626q
Kayat J, Gajbhiye V, Tekade RK, Jain NK (2011) Pulmonary toxicity of carbon nanotubes: a systematic report. Nanomed Nanotechnol Biol Med 7:40–49. doi:10.1016/j.nano.2010.06.008
Lanone S, Andujar P, Kermanizadeh A, Boczkowski J (2013) Determinants of carbon nanotube toxicity. Adv Drug Deliv Rev 65:2063–2069. doi:10.1016/j.addr.2013.07.019
Leshuai W, Zhang LZ (2007) Biological interactions of functionalized single-wall carbon nanotubes in human epidermal keratinocytes. Int J Toxicol 26:103–113. doi:10.1080/10915810701225133
Liu X, Sen S, Liu J et al (2011) antioxidant deactivation on graphenic nanocarbon surfaces. Small 7:2775–2785. doi:10.1002/smll.201100651
Lynch I, Dawson KA (2008) Protein–nanoparticle interactions. Nano Today 3:40–47. doi:10.1016/S1748-0132(08)70014-8
Mahdi AA, Tripathi S, Neerja J, Hasan M (2010) Aluminium mediated oxidative stress: possible relationship to cognitive impairment of Alzheimer's type. Ann Neurosci 13:18–24. doi:10.5214/112
Mao H, Chen W, Laurent S et al (2013) Hard corona composition and cellular toxicities of the graphene sheets. Colloids Surf B Biointerfaces 109:212–218. doi:10.1016/j.colsurfb.2013.03.049
Muller J, Huaux F, Moreau N et al (2005) Respiratory toxicity of multi-wall carbon nanotubes. Toxicol Appl Pharmacol 207:221–231. doi:10.1016/j.taap.2005.01.008
Muller J, Huaux F, Fonseca A et al (2008) Structural defects play a major role in the acute lung toxicity of multiwall carbon nanotubes: toxicological aspects. Chem Res Toxicol 21:1698–1705. doi:10.1021/tx800101p
Nagai H, Okazaki Y, Chew SH et al (2011) Diameter and rigidity of multiwalled carbon nanotubes are critical factors in mesothelial injury and carcinogenesis. Proc Natl Acad Sci USA 108:E1330–E1338. doi:10.1073/pnas.1110013108
Peigney A, Laurent C, Flahaut E et al (2001) Specific surface area of carbon nanotubes and bundles of carbon nanotubes. Carbon 39:507–514. doi:10.1016/S0008-6223(00)00155-X
Pinault M, Mayne-L'Hermite M, Reynaud C et al (2004) Carbon nanotubes produced by aerosol pyrolysis: growth mechanisms and post-annealing effects. Diam Relat Mater 13:1266–1269. doi:10.1016/j.diamond.2003.12.015
Porter DW, Hubbs AF, Mercer RR et al (2010) Mouse pulmonary dose- and time course-responses induced by exposure to multi-walled carbon nanotubes. Toxicology 269:136–147. doi:10.1016/j.tox.2009.10.017
Rakotomalala R (2005) TANAGRA: un logiciel gratuit pour l'enseignement et la recherche. RNTI-E-3, pp 697–702
Ruipérez F, Mujika JI, Ugalde JM et al (2012) Pro-oxidant activity of aluminum: promoting the Fenton reaction by reducing Fe(III) to Fe(II). J Inorg Biochem 117:118–123. doi:10.1016/j.jinorgbio.2012.09.008

Schinwald A, Murphy FA, Prina-Mello A et al (2012) The threshold length for fiber-induced acute pleural inflammation: shedding light on the early events in asbestos-induced mesothelioma. Toxicol Sci 128:461–470. doi:10.1093/toxsci/kfs171

Schrurs F, Lison D (2012) Focusing the research effort. Nat Nanotechnol 7:546–548

Shvedova AA, Kisin E, Murray AR et al (2008) Inhalation vs. aspiration of single-walled carbon nanotubes in C57BL/6 mice: inflammation, fibrosis, oxidative stress, and mutagenesis. Am J Physiol Lung Cell Mol Physiol 295:L552–L565. doi:10.1152/ajplung.90287.2008

Shvedova AA, Kisin ER, Porter D et al (2009) Mechanisms of pulmonary toxicity and medical applications of carbon nanotubes: two faces of Janus? Pharmacol Ther 121:192–204. doi:10.1016/j.pharmthera.2008.10.009

Shvedova AA, Pietroiusti A, Fadeel B, Kagan VE (2012) Mechanisms of carbon nanotube-induced toxicity: focus on oxidative stress. Toxicol Appl Pharmacol 261:121–133. doi:10.1016/j.taap.2012.03.023

Simon-Deckers A, Gouget B, Mayne-L'Hermite M et al (2008) In vitro investigation of oxide nanoparticle and carbon nanotube toxicity and intracellular accumulation in A549 human pneumocytes. Toxicology 253:137–146. doi:10.1016/j.tox.2008.09.007

Tsukahara T, Haniu H (2011) Cellular cytotoxic response induced by highly purified multi-wall carbon nanotube in human lung cells. Mol Cell Biochem 352:57–63. doi:10.1007/s11010-011-0739-z

Vietti G, Ibouraadaten S, Palmai-Pallag M et al (2013) Towards predicting the lung fibrogenic activity of nanomaterials: experimental validation of an in vitro fibroblast proliferation assay. Part Fibre Toxicol 10:52

Wörle-Knirsch JM, Pulskamp K, Krug HF (2006) Oops they did it again! Carbon nanotubes hoax scientists in viability assays. Nano Lett 6:1261–1268. doi:10.1021/nl060177c

Xia W, Wang Y, Bergsträßer R et al (2007) Surface characterization of oxygen-functionalized multi-walled carbon nanotubes by high-resolution X-ray photoelectron spectroscopy and temperature-programmed desorption. Appl Surf Sci 254:247–250. doi:10.1016/j.apsusc.2007.07.120

Yamamoto G, Shirasu K, Nozaka Y et al (2013) Structure–property relationships in thermally-annealed multi-walled carbon nanotubes. Carbon. doi:10.1016/j.carbon.2013.08.061

Zhang X, Zhu Y, Li J et al (2011) Tuning the cellular uptake and cytotoxicity of carbon nanotubes by surface hydroxylation. J Nanoparticle Res 13:6941–6952. doi:10.1007/s11051-011-0603-9